Geomechanics and Engineering, *Vol. 33, No. 5 (2023) 439-451*
https://doi.org/10.12989/gae.2023.33.5.439

Characterization of face stability of shield tunnel excavated in sand-clay mixed ground through transparent soil models

YuanHai Li[1,2], XiaoJie Tang*[1,2], Shuo Yang[3] and YanFeng Ding[1,2]

[1]*State Key Laboratory for Geomechanics and Deep Underground Engineering, Xuzhou, China*
[2]*School of Mechanics and Civil Engineering, China University of Mining and Technology, Xuzhou, China*
[3]*School of Civil Engineering, Xuzhou University of Technology, Xuzhou, China*

(*Received August 24, 2022, Revised February 10, 2023, Accepted March 16, 2023*)

Abstract. The construction of shield tunnelling in urban sites is facing serious risks from complex and changeable underground conditions. Construction problems in the sand-clay mixed ground have been more reported in recent decades for its poor control of soil loss in tunnel face, ground settlement and supporting pressure. Since the limitations of observation methods, the conventional physical modelling experiments normally simplify the tunnelling to a plane strain situation whose results are not reliable in mixed ground cases which exhibit more complicated responses. We propose a new method for the study of the mixed ground tunnel through which mixed lays are simulated with transparent soil surrogates exhibiting different mechanical properties. An experimental framework for the transparent soil modelling of the mixed ground tunnel was established incorporated with the self-developed digital image correlation system (PhotoInfor). To understand better the response of face stability, ground deformation, settlement and supporting phenomenon to tunnelling excavation in the sand-clay mixed ground, a series of case studies were carried out comparing the results from cases subjected to different buried depths and mixed phenomenon. The results indicate that the deformation mode, settlement and supporting phenomenon vary with the mixed phenomenon and buried depth. Moreover, a stratigraphic effect exists that the ground movement around mixed face reveals a notable difference.

Keywords: digital image correlation; face stability; modelling experiment; sand-clay mixed ground; shield tunnel; transparent soil

1. Introduction

Shield tunnelling has been widely used as a safe and efficient method in underground construction. Particularly, earth pressure balance (EPB) tunnelling has an absolute advantage in tunnelling practice due to its technical and economic features (Galli and Thewes 2019, Lemer 1997).

The development of underground construction in wide cities is currently facing serious risks from complex and changeable underground conditions (Chen *et al.* 2016, Zhang *et al.* 2020, Zhang and Huang 2014). Particularly, EPB construction in the mixed ground has been a typical situation where considerable engineering problem was caused (Vergara and Saroglou 2017, Xie *et al.* 2018, Zhao *et al*. 2019). Under this condition, the weak ground around the mixed face is easy to be over-excavated which can induce abnormal movement of the soil around the tunnel face, resulting in abnormal ground deformation and excessive settlement (Wang *et al*. 2021). Meanwhile, tunnel collapse, water inrush, and shield jam have been regularly reported as well which pose a huge threat to both construction safety and the natural environment (Cui *et al.* 2016, Hasanpour *et al.* 2017, Liu *et al.* 2020, Xu *et al.* 2021, Xue *et al*. 2019). How to ensure the safety of engineering for tunnelling under mixed ground conditions has been a heated topic in relevant research.

Engineering problems encountered in areas with the mixed ground are tightly related to geological characteristics. Mixed ground constitutes the simultaneous presence of two or more geological materials on the tunnel face that exhibit significantly different material properties (Tóth *et al.* 2013). The normally encountered mixed situation is rock-rock, soil-rock and soil-soil combined cases in which the latter two cases which exhibit soft-top and hard-bottom characteristics are most frequently met in urban underground construction. Sand-clay mixture is a common situation in the soil-soil mixed ground. During the construction of the EPB shield under such conditions, due to the large difference in mechanical properties between the upper sand and the lower clay, the intensity of the disturbance affected by the excavation of shield tunnelling is different in the respective ground region around the tunnel face. Therefore, the pressure of the soil bin at the tunnel face is difficult to control under such conditions, which normally induces a large quantity of soil loss and an extremely unstable tunnel face (Ma *et al*. 2015, Yang *et al.* 2016).

The deformation mode or the shape of the damage zone of the shield tunnel in the mixed ground has been unclear which is one of the core contents in the study of tunnelling instability and provides an important base for assumptions

*Corresponding author, Ph.D.
E-mail: tangxiaojie_edu@163.com

ISSN: 2005-307X (Print), 2092-6219 (Online)

in theoretical analysis of the limit analysis and the limit equilibrium calculation. The deformation mode of the shield excavation surface is mostly studied through observation in physical modelling experiments. With the help of numerical solutions, the research method in recent decades has been extended to the discrete element method, finite element method, etcetera (Alagha and Chapman 2019, Wang *et al*. 2022, Zhang *et al*. 2015). Under uniform ground conditions, the growth of the damage zone in clay ground has been experimentally investigated showing a characteristic that the damaged area around the tunnel face originates close to the bottom of the tunnel, and gradually extends to the ground surface, and finally exhibits a funnel-like collapse. While in the sandy ground, the damage zone shows a chimney-like region (Meguid *et al.* 2008). However, the shape of the damage zone, as well as its evolution under mixed ground conditions, has been less investigated experimentally. The main difficulty lies in its complex ground condition to be modelled in the laboratory environment and the limitation of observation methods for internal conditions. For tunnelling under the mixed ground condition which exhibits inhomogeneous characteristics, the accurate observation of the deformation mode around the tunnel face is the premise and basis for the study of instability mechanism. The conventional modelling experiments through opaque materials fail to reach the internal deformation which brings difficulty for direct identification of failure modes. In replace, numerical solutions can overcome the conundrum in physical modelling experiments in terms of internal observation (Hayashi *et al.* 2022), however whose proper settlement of material properties and the selection of suitable constitutive models calls for attentive adjustment. Accordingly, most experimental practice degrades the tunnelling to a plane strain situation which ignores the deformation perpendicular to the tunnel face (Li *et al.* 2019). Such simplification is not reliable under conditions whose ground thickness varies along the direction of tunnelling. Moreover, the mixed ground can induce a more complicated phenomenon of ground movement as the progress of excavation, which calls for the observation with a three-dimensional approach for visualization of the internal situation.

To reach direct observation of deformation mode of shield tunnel excavated in the sand-clay mixed ground, we developed a new solution simulating the complicated ground with multiple kinds of transparent soil surrogates exhibiting distinct mechanical properties. The evolution of transparent synthetic materials enables the study of spatial behaviours and flow features inside the soil (Ganiyu *et al*. 2016, Sun and Liu 2014, Zhang *et al*. 2020) when coupled with optical measuring methods and image processing techniques such as digital image correlation (DIC) and particle image velocimetry (PIV) (Keating *et al*. 1975, Li and Einstein 2017, Liu and Iskander 2004). In our work, the sand-clay mixed ground condition was simulated with two kinds of transparent materials fabricated in layers that were subjected to different consolidation treatments. The transparent state of materials enables the observation of ground conditions around the tunnel based on which the internal measurement can be realized via non-contact testing systems. The DIC method was utilized here for the measurement of deformation through our self-developed image-processing software- PhotoInfor (Li *et al.* 2016, Li *et al.* 2020, Li *et al*. 2022, Zhang *et al*. 2012).

To further understand the response of ground deformation, settlement and supporting phenomenon to the EPB shield tunnelling excavated in the mixed ground, a series of modelling experiments were carried out comparing the results from cases subjected to different buried depths and mixed phenomenon throughout the excavation. In sections to come, we first lay out the preparation details of transparent soil surrogates as well as mechanical properties, followed by a detailed description of the setup of modelling experiments. Thereafter, the experimental results are compared in groups to conclude the variation of damage zone under complex ground conditions through the direct observation and measurement of internal soils.

2. Preparation of transparent soil surrogates

2.1 Material composition

To simulate the mixed ground condition with transparent materials, two kinds of soil surrogates are required for sand and clay ground, respectively. Based on previous work and our testing results, transparent soil surrogates should be made of the skeleton material and void fluid in composition. For the sake of optical tests via the DIC, two kinds of compounds (skeleton and fluid) are required to exhibit a close refractive index in the final state. In our practice, we follow a solution adjusting the ingredient of void fluid to match the index of skeleton material.

As for the simulated sand ground, the skeleton of composite material was selected as fused quartz sands for its high purity and transparency whose particle size used for experiments ranges from 0.5 to 1.0 mm. The physical properties were tested for elastic module of 72 GPa, density of 2.65 g/cm^3, Mons hardness scale of 7 and refractive index (RI) of 1.4585. To match the RI of the skeleton, the components of the void fluid, as well as the corresponding volume ratio, were tested in trials. The mixed fluid of n-Dodecan ($CH_3(CH_2)_{10}CH_3$) and white oil has been tested to reveal a similar RI of 1.4585 with a volume ratio fixed at 1: 4, hence suitable to be mixed with the skeleton material. Noted here the RI was tested with the Abbe refractometer after the stirring to a uniform state.

According to Hird (2010), the transparent clay prepared with hydrated silica has higher transparency and a clearer speckle field than that with amorphous silica powder. The skeleton material for simulated clay ground was selected as hydrated silica ($SiO_2.nH_2O$) whose average particle size used for experiments is less than 15 μm. The refractive index of hydrated silica was tested at 1.442 which is close to that for simulated sand, due to which the void fluid for simulated clay ground remained the same as the former one.

Two kinds of transparent material underwent similar steps in early-stage preparation. It started with the mixing of skeleton material and void fluid in a model box followed by vacuuming for 30 minutes to expected transparency. As

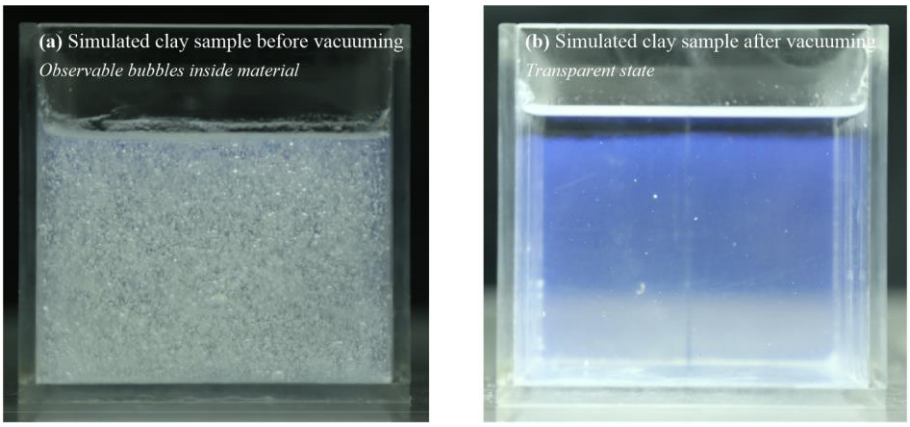

Fig. 1 Simulated clay sample before and after the vacuuming. The sample in (a) after the mixture calls for necessary vacuuming to remove bubbles for a transparent state

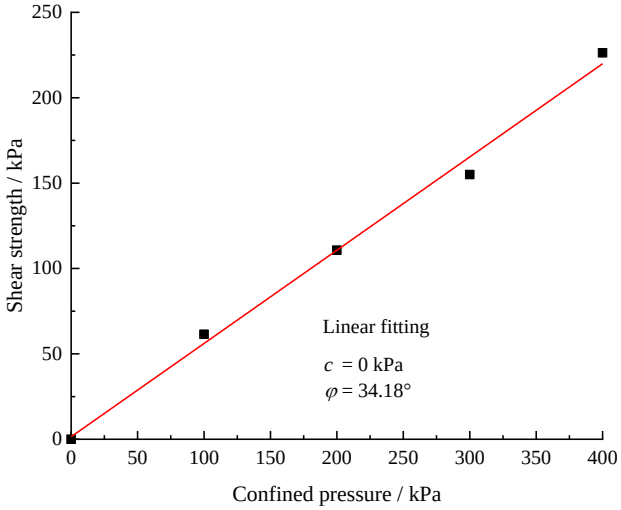

Fig. 2 Shear strength of transparent sand. The material composed of fused quartz and the composite oil shows poorly cohesive characteristics which are suitable for modelling sand

shown in Fig. 1(a), the vacuuming treatment is more necessary for simulated clay due to more bubbles generated inside after the mixing. The transparent sand can be harvested after another 1 hour of stabilization. However, the preparation of clay material calls for additional consolidation to reach a cohesive state. Noted here the model box for transparent clay was set with an adjusted porous base for oil drainage under the loading.

2.2 Mechanical properties

After the preparation of transparent soil surrogates including simulated sand and clay, direct shear tests were carried out for the measurement of cohesion and friction angle. As shown in Fig. 2, the friction angle of transparent sand was tested as 34.18° and the cohesion strength was zero indicating a poorly cohesive characteristic suitable for the simulation of sand ground.

The property of transparent clay is related to the treatment of pre-consolidation. Firstly, the oil content is changeable when the material is subjected to pre-consolidation with different pressure. As shown in Fig. 3(a), the oil content reveals an exponentially decreasing trend as the increment of pre-consolidation pressure, the law of which is instructional to the preparation of transparent clay. The strength surfaces of transparent clay in six pre-consolidation conditions are depicted in Fig. 3(b). It is shown that the transparent clay subjected to a larger value of pre-consolidation reveals a higher strength surface indicating a hardening characteristic that is suitable for the modelling of clay material.

As for 6 groups of pre-consolidation tests, we have a set of cohesion and friction angle data, that are (5.15 kPa, 15.8°), (6.32, 17.2°), (8.5 kPa, 21.6°), (13.2 kPa, 22.2°), (15.1 kPa, 24.1°) and (18.2 kPa, 24.5°) respectively corresponding to six increased consolidation pressures. To simulate the clay ground with comparatively similar mechanical properties, the analogical clay subjected to a pre-consolidation pressure of 12.5 kPa was selected for the simulation of clay ground in experiment. The results of the consolidation test are shown in Fig. 4 in which the compressibility coefficient a_{1-2} (a factor derived with corresponding data at $p_1 = 100$ kPa and $p_2 = 200$ kPa respectively) of transparent clay is calculated as 1.38 MPa^{-1} showing a characteristic of high compressibility.

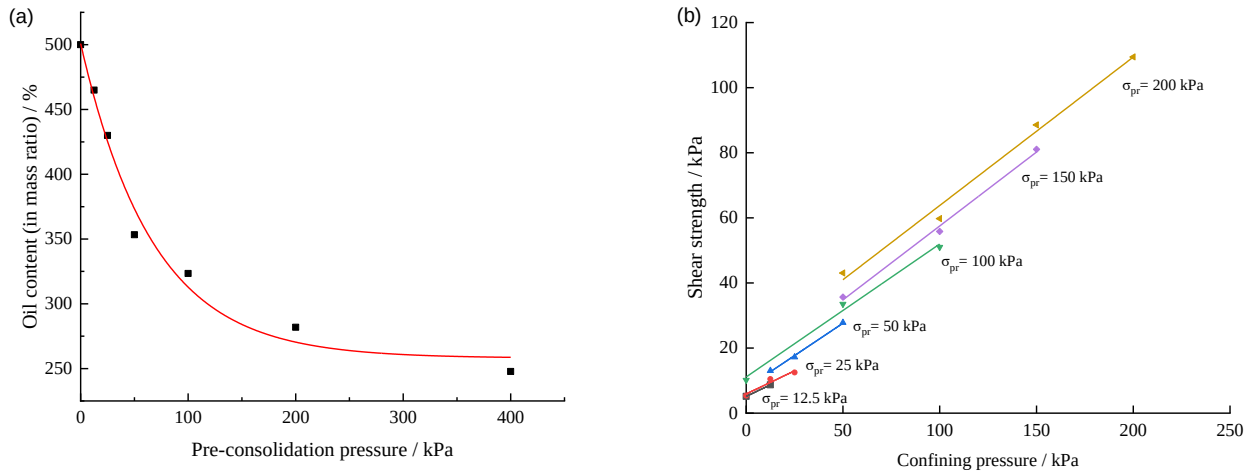

Fig. 3 (a) The evolution of the oil content in transparent clay as the change of pressure for pre-consolidation treatment (in expositional fitting) and (b) The strength surfaces of transparent clay under six pre-consolidation conditions

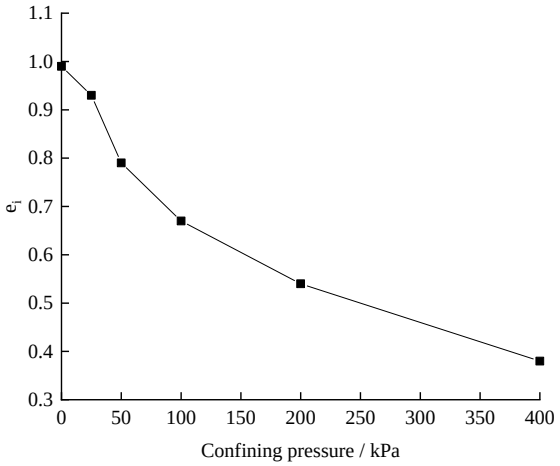

Fig. 4 The curve of compressibility behaviour

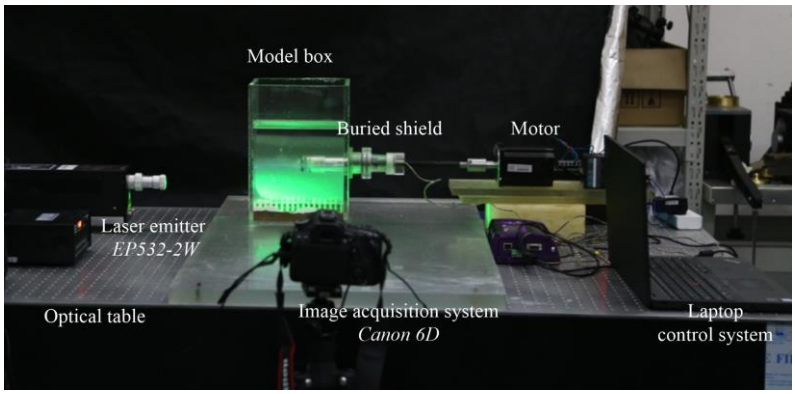

Fig. 5 Experiment set-up for modelling of shield tunnel excavated in transparent materials

3. Modeling experiment

3.1 Set-up

As depicted in Fig. 5, the experimental setup consists of self-developed excavation equipment for the modelling of shield tunnel in transparent materials, a pressure cell set on the shield tunnel, a laser face emitter for the observation of speckle pattern for optical tests, and an image acquisition equipment for monitoring of deformed ground.

The shield model, as shown in Fig. 6, is composed of a movable shield in the head, a plexiglass shell, connecting shaft in the centre and a sealing ring. The tunnel head made of polycarbonates is 36 mm in diameter and 25 mm in length which is connected with a threaded shaft in the

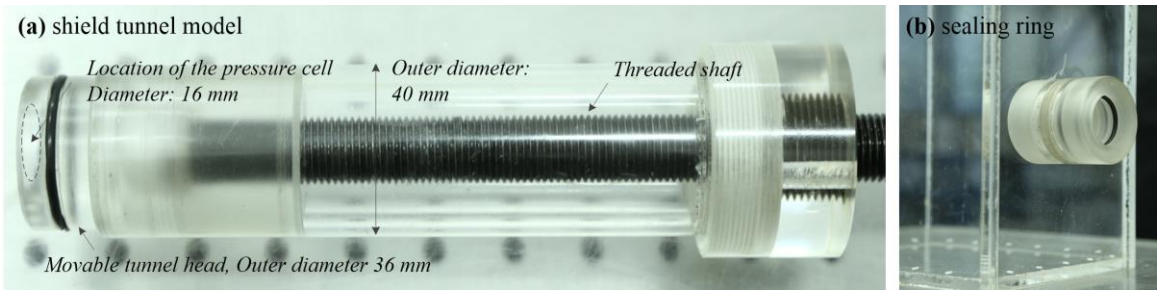

Fig. 6 The model of the shield tunnel made up of the movable tunnel head, connected shaft, and sealing ring fixed on the model box

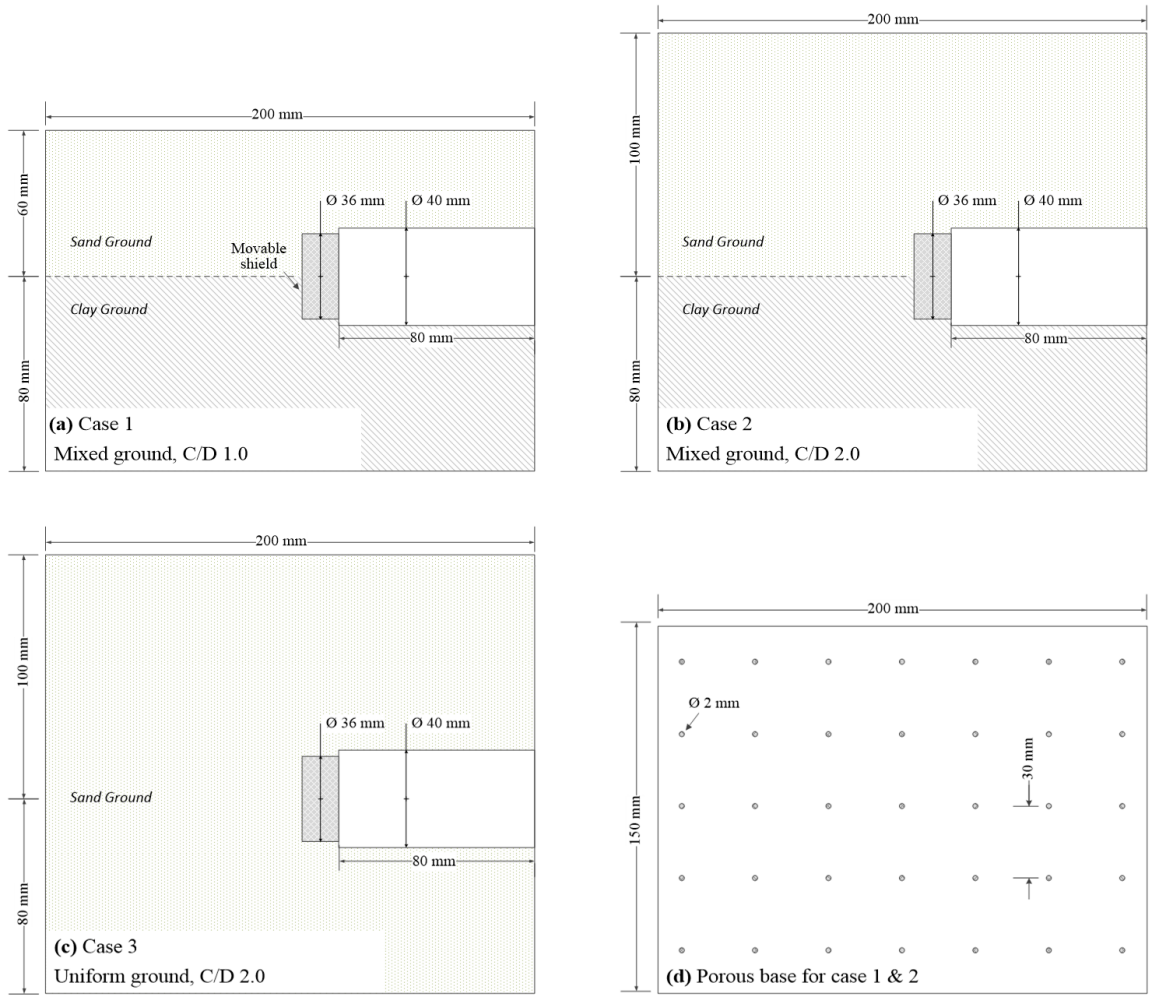

Fig. 7 Schematic of shield model excavated under multiple ground conditions and buried depth. (a) ~ (c) depicts the front view of the model in three respective cases. (d) shows the base of the model box of case 1 and case 2 where porous holes were prepared for drainage during the consolidation of simulated clay material

centre. A circular hole with a diameter of 16 mm and a thickness of 4.8 mm is manufactured at the centre of the front panel of the head for the installation of the pressure cell. The movement of the tunnel head is driven by the motor control system (MTPG2) whose step length, number of segments, the direction of the rotation can be adjusted.

The buried shell is a hollow cylinder with an outer diameter of 40 mm which is fixed to the model box to prevent the upper material from collapsing and to provide protection for the movement of the supporting panel. The connection at the model box is designed with a threaded ring to stabilize the excavation model and to prevent the leakage of transparent material as shown in Fig. 6(b).

3.2 Experiment schemes

Three cases studying influence factors of buried depth and mixed conditions were carried out in this work (see Fig. 7). Two buried conditions were investigated that a height of 40 mm (C/D 1.0) for sand ground represented a shallow-

(a) transparent clay (b) transparent sand

Fig. 8 Creation of speckle pattern for optical measurement in simulated sand and clay materials, respectively. (a) Half of the transparent clay is mixed with tracer particles for speckles inside and (b) Speckle patterns can be created in transparent sand under irradiation from a laser light without any additional mixture

buried condition (case 1) while 80 mm (C/D 2.0) for a deeper buried condition (case 2), relatively. The mixed ground composed of simulated sand and clay was fabricated for every two cases in which the buried depth was denoted by the thickness of sand ground above the upper surface of the tunnel. Meanwhile, case 3 under a uniform ground condition (simulated sand material) was conducted for comparison whose buried depth was the same as the deeply buried case. Noted here, as depicted in Fig. 7(d), cases 1 and 2 have a porous base for drainage during consolidation for simulated clay, and case 3 has the same-size base without any drainage holes.

In the present experiment, the gravitational acceleration ratio C_g is out of our concern since experiment limitations. The strength and density between analogue material and real ground remain similar contributing to similarities $C_\sigma = C_\rho = 1$. According to shield size in practical work, the geometric similarity ratio is set as 500 (C_L=500), and the time similarity ratio can be calculated as C_t=22.4 based on scaling laws (Li *et al*. 2019).

3.3 Fabrication of ground layers

As described above, for mixed ground case, the ground layer consists of two kinds of transparent material around a shield tunnel of radius 20 mm. The size of transparent clay, buried below, is 200 mm, 150 mm, 80 mm in length, width, and height. The height of the sand ground is a case factor dependent on the buried depth as described above. In what follows, we present the details of how we fabricated the ground layer in the model box and created the speckle pattern for the DIC analysis.

Tracer particles (Titanium Oxide) were mixed with the transparent clay for speckle patterns and the mass ratio of titanium oxide against white silica was fixed at 0.015% in this experiment. Noted here, as shown in Fig. 8(a), the mixed clay has much lower transparency due to which only the half material on the backside of the observation face was mixed with the tracer. As depicted in Fig. 8(b), a speckle field can be created under laser irradiation for transparent sand, hence no additional tracer is added accordingly.

Fig. 9 depicts the final observation face of the mixed ground and the buried tunnel under the irradiation of laser light. The procedure for the fabrication of the mixed ground is divided into three stages including the setup of the clay ground, buried tunnel and the sand ground in sequence. Firstly, the prepared transparent clay is separated into two parts and one of them is mixed with tracer particles for DIC measurement. Two kinds of prepared clay with a certain volume are poured into respective spaces in the box which is divided via a thin sheet in the middle. The vacuuming treatment is followed for 30 minutes after which the shield model can be buried into the ground followed by a sealing check. To realize a cohesive state for transparent clay, we took out the sheet and carried out the consolidation in several steps to a final loading of 12.5 kPa. What comes followed is the preparation of the sand ground. The mixed fluid made from n-Dodecan and white oil was poured into the box above the clay surface followed by the sprinkle of fused quartz sand at a specific ratio. It should be noted here the fabrication of the whole sand ground was separated into four layers for a uniform state. Finally, the model ground was exposed to vacuuming for another 10 minutes to remove bubbles inside, after which the mixed ground was well prepared with a speckled pattern on the observation face.

3.4 Experiment procedures

Firstly, the environment of temperature, brightness and humidity which affects the experimental results was adjusted and controlled before the settlement of the experimental setup. The prepared model box, as well as the connected excavation system, was then fixed on the optical table to avoid vibration. Thereafter, the laser system was activated to create a laser face across the transparent material followed by the focusing of the camera. As illuminated via a laser generator (EP532-2W), a plane surface with a speckled pattern in the material was monitored with Canon 6D (5472×3648 pixels in resolution) throughout the experiment. All of the equipment including the excavation motor, camera and pressure transducer were connected to a laptop with an appropriate set of parameters.

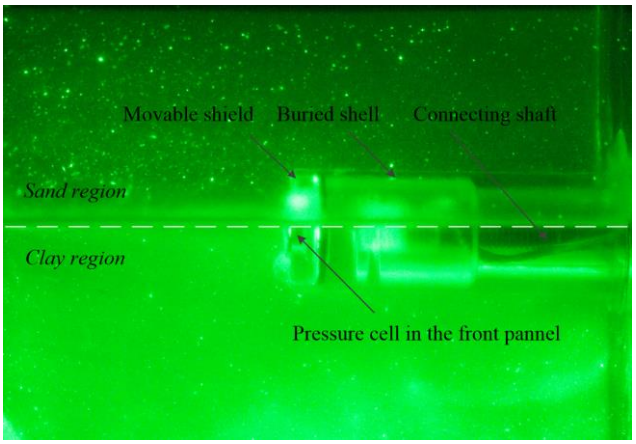

Fig. 9 The observation face of the mixed ground and the buried tunnel under the irradiation of laser. The observation face with a clear speckle pattern can be well monitored via the camera and transparent material on the front side shows little influence on image acquisition

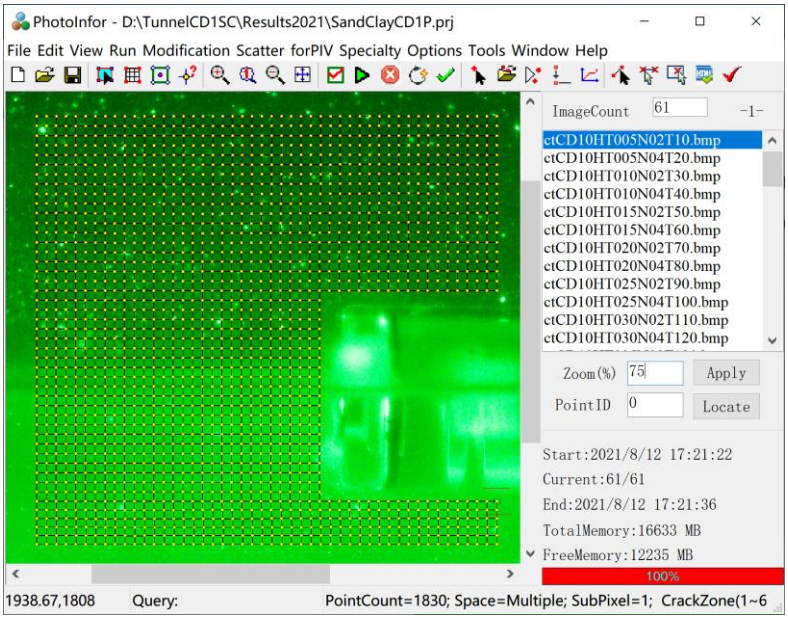

Fig. 10 The interface of the processing software (PhotoInfor) for DIC. Self-developed software named PhotoInfor is used in the experiment

The shooting speed of the camera was set at 5 seconds and the pressure data is collected by second throughout the whole experiment.

Upon the preparation work being completed, the camera and pressure cell started working followed by the activation of the motor. The shield moves back controlled by the motor. Noted here the supporting phenomenon of shield tunnel in the soil layer is generally modelled by controlling the backward movement of the shield panel. This practice in our work is reasonable for the modelling of the unloading effect of the shield tunnel excavated in the soft soil layer. The shield moves backwards 0.5 mm after each rotation of 90 degrees of the connecting shaft within 10 seconds. After the working of the motor for every 10 seconds, the shield held still for another 10 seconds before the next moving. Four images will be taken for each excavation process within 20 seconds. The excavation of the shield stops running until a final distance of 20 mm.

3.5 Optical measurement through DIC

Digital speckle correlation testing was conducted afterwards for the measurement of deformation at the observation surface. Self-developed PhotoInfor (Li *et al.* 2022), a speciality DIC software, was used here for image correlation analysis whose working interface is shown in Fig. 10. PhotoInfor can be used for image analysis and displacement calculations through a correlation calculation formula, and strain calculations, coordinate conversions, and sub-pixel analysis can all be realized based on the FEM method. Noted that the appropriate setting of DIC parameters is important to achieve an accurate result. After a series of adjusting tests, the block size, subset interval and searching radius were set at 81, 20 and 10 pixels for all case studies. It should be noted here the mesh boundary was kept a small distance to (no touching) the shield surface and upper ground surface to avoid the computation error in DIC.

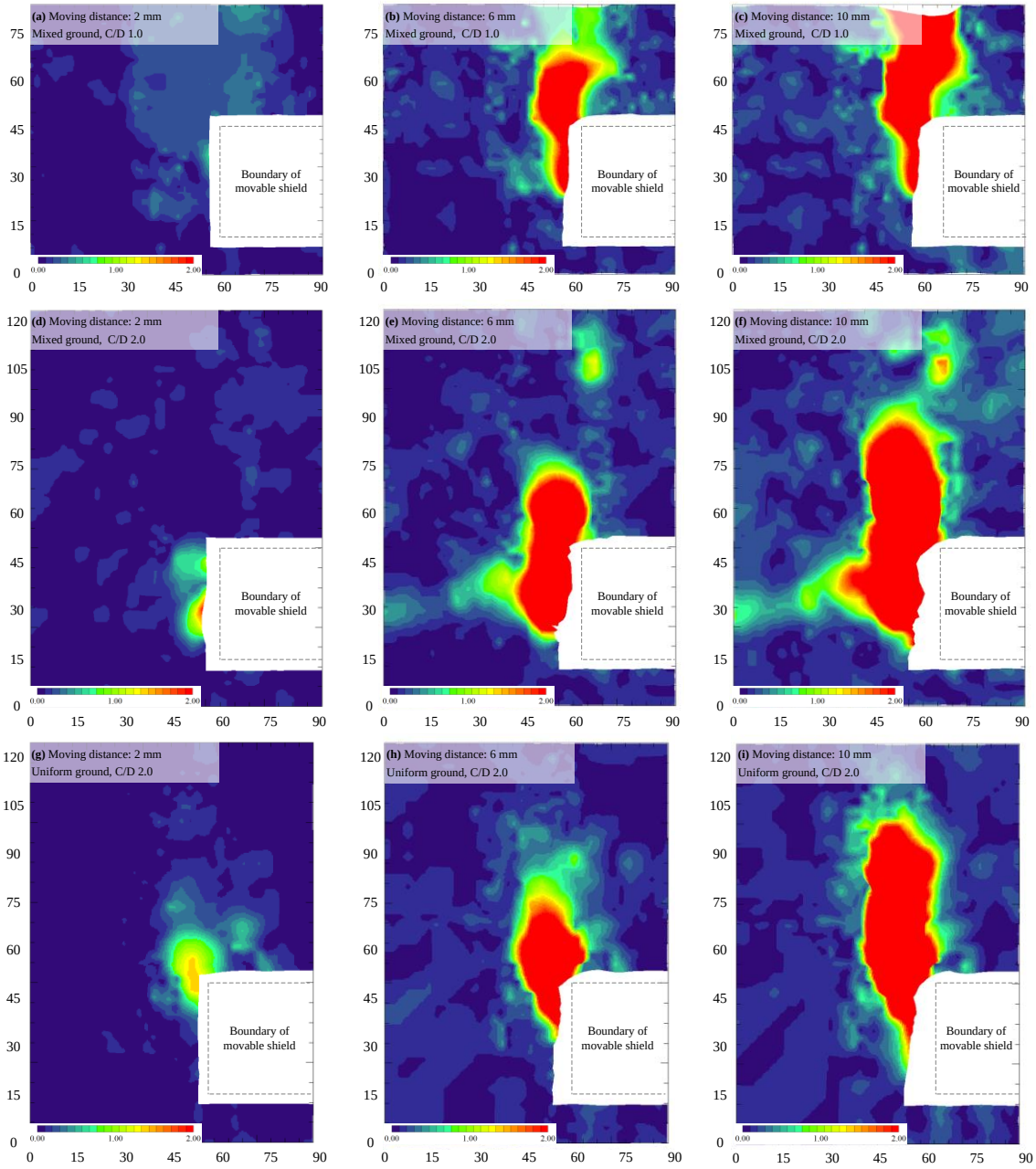

Fig. 11 Diagram of displacement magnitude measured through DIC throughout the excavation process in three cases. (a)-(c) show the phenomenon with the shallow-buried condition of the mixed ground case while (d)-(f) represent the deep-buried condition, and (g)-(i) depict the case of uniform ground. Noted that the unit of the coordinate and legend is in millimetres

4. Results

In this section, we present the results of experiments in which we explore the characteristics of ground deformation in three cases. The deformation mode represented by the concentrated region of the ground movement was further concluded based on the diagram of displacement vectors. In what followed, the settlement and the supporting phenomenon at tunnel face were studied in mixed-ground cases. Finally, the stratigraphic effect was analyzed and illustrated by the difference-ratio of displacement magnitude around the mixed face.

4.1 Ground deformation

Diagram of displacement magnitude measured through DIC is depicted in Fig. 11 where (a)-(c) show the phenomenon under the shallow-buried condition in the mixed ground case and (d)-(f) represent the deep-buried condition. (g)-(i) depicts the case of uniform ground. The position where the observable ground movement originates and the distribution as well as the evolution of concentrated area in ground movement vary a lot with the ground condition and buried depth.

As the movement of shied, the pressure at the tunnel

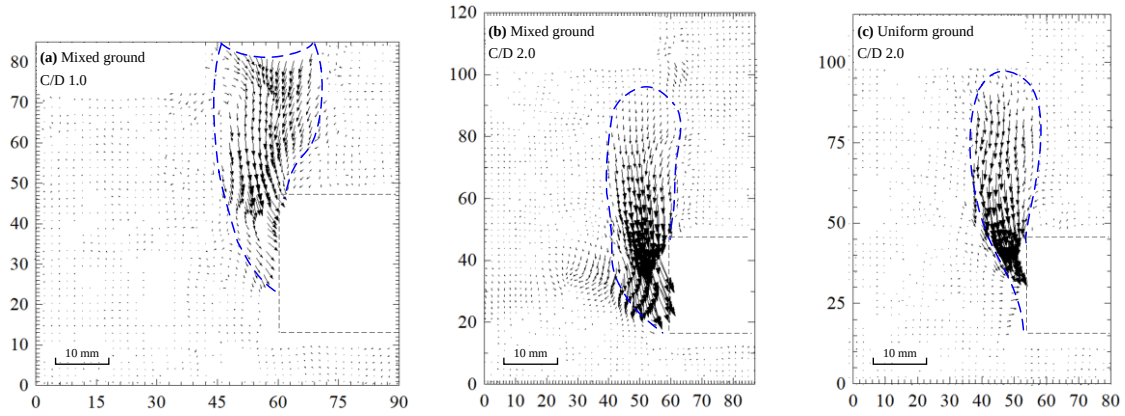

Fig. 12 Deformation modes of tunnels varied with the mixed condition and buried depth. (a) A shallow-buried tunnel excavated in mixed ground condition, (b) A deep-buried tunnel excavated in mixed ground condition and (c) A deep-buried tunnel excavated in uniform ground condition. The vectors in the figures denote the phenomenon of ground displacement. Noted that the unit of the coordinate is in millimetres

head dropped a lot simulating the excavation face lack of acting pressure. As depicted in Figs. 11(a), 11(d) and 11(g), the localized displacement occurs at the top of the tunnel face firstly. As for the excavation in the mixed ground under the deep-buried condition, the region around the mixed face reveals notable displacement concentration as well compared with the other two cases since the combined action of higher ground pressure and inhomogeneous properties due to the mixed condition.

As the excavation proceeded, the arch effect takes place in three cases. The collapse originates at the tunnel vault in the sandy region and gradually extends to the ground surface as the shield movement. It should be noted that the observable collapse in the shallow-buried case first spreads to the ground surface after the shield movement of 6 mm. As shown in Fig. 11(c), the ground surface reveals a significant settlement indicating a dangerous signal to the architecture on the ground. In comparison, the concentrated ground movement in the other two deep-buried cases (mixed and uniform ground) never extend to the surface area showing that the damage of the excavated surface may not develop to the ground when the buried depth is large enough due to the effect of soil arching, but only appears as partial damage. In our work, we experimentally show this situation exists also in tunnelling under mixed ground conditions.

The deformation modes in respective cases represented by a concentrated area of ground movement are shown in Fig. 12. As for the excavation in the mixed ground at shallow buried condition, the damage zone exhibits a funnel-like shape that the top of the funnel touches the ground surface, and the bottom is a little above the tunnel boundary. In this case, as the movement of shield, the unconsolidated sand above the mixed face flows into the gap and induces the settlement region. Meanwhile, the clay buried below exhibits harder characteristics and holds the position during the process, since which the funnel did not extend to the tunnel bottom.

However, as the buried depth increased followed by a higher ground pressure, the bottom of the funnel extends to a deeper position as depicted in Fig. 12(b). It should be noted that the clay region underwent a further ground movement in front of the tunnel face. Meanwhile, for the deep buried case (b) and (c), the shape of the funnel top indicates the existence of soil arching. After the excavation of tunnel in deep buried ground, the upper sand tends to be loosened and starts to flow inside. In such a case, the occurrence of soil arching redistributes the pressure in upper sandy ground and stops the continued ground movement. A funnel-like damage zone emerges afterwards. As depicted in Fig. 12(c) the mode of the uniform-ground case shows a conventional funnel that the bottom touches the boundary of the tunnel boundary and the material inside the damage funnel shows a potential flowing into the gap agreeing well with the relevant research (Chambon and Corte 1994, Chen *et al*. 2011, Leca and Dormieux 1990). In both two cases, the funnel top never extends to the ground surface in comparison with the shallow buried case due to soil arching.

4.2 Settlement

Under the mixed ground condition, the buried depth plays a role in the situation of ground settlement. Fig. 13 depicts the phenomenon of ground settlement under two buried conditions at three excavation steps. Noted here the data of ground settlement is distributed over the line parallel with the excavation direction rather than the route perpendicular. Since asymmetrical ground movement, as indicated by Fig. 12, the settlement in front of and behind the excavation surface is asymmetrical. Firstly, as the excavation proceeded, the ground surface under the shallow-buried condition reveals an observable development in the settlement that the largest vertical displacement in the ground surface reaches -0.192, -0.896, and -3.328 mm as the moving distance reaching 2, 6, and 10 mm, respectively. At the same timesteps, the settlement value in the deep-buried condition fluctuates within a range from -0.25 to 0.25 mm, indicating a comparatively weaker influence from the excavation since the soil arching extends little to the surface. It should be noted that the largest settlement occurs at the position around the original tunnel face where the soil arching originates.

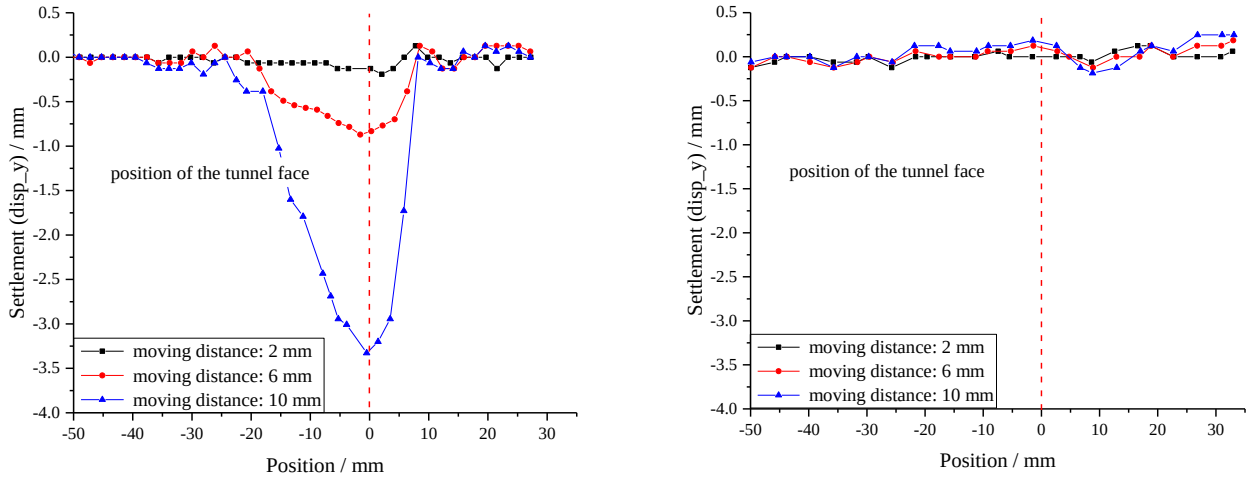

(a) shallow-buried case (C/D 1.0) (b) deep-buried case (C/D 2.0)

Fig. 13 Ground settlement under mixed ground condition. (a) The shallow-buried condition shows an observable development of settlement around the position of the tunnel face and (b) Excavation in the deep-buried condition reveals a weaker influence on settlement

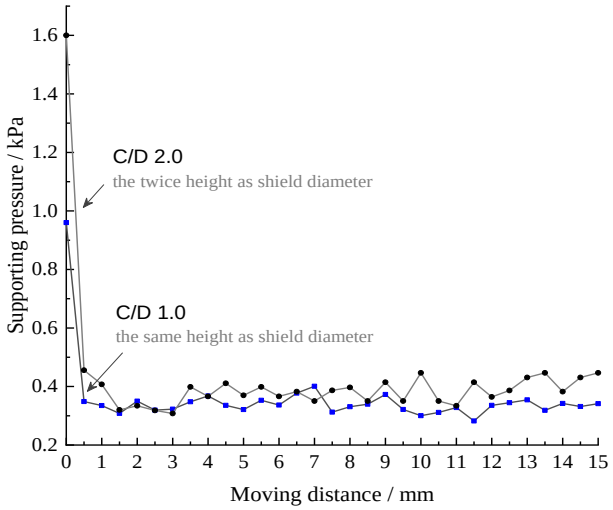

Fig. 14 Evolution of the supporting pressure at the tunnel face in two tunnels with different buried depths. The buried depth influences a lot the supporting pressure at the initial stage, the duration of pressure dropping and the value in the latter process

4.3 Support phenomenon at the tunnel face under the mixed ground condition

The evolution of the supporting pressure in the tunnel face was monitored through the pressure cell set at the shield head. As depicted in Fig. 14, the buried depth influences a lot the value initially that the tunnel excavated at a depth of 40 mm in this experiment undertakes a pressure of 0.96 kPa while the data shows 1.6 kPa under the condition with a twice depth. As the movement of shield, the pressure for supporting drops sharply in two cases since the release of the ground compression. Noted that for cases with a deeper buried depth, the pressure falls at a higher speed and its dropping sustains a further ground movement indicating a worse phenomenon of the tunnel lacking supporting pressure. After the moving distance approaching 0.5 mm, the tunnel surface in the case with a buried depth of 40 mm reaches an approximate stable pressure for supporting at 0.35 kPa. However, another case (80 mm depth) shows an ongoing dropping until the moving distance of 1.5 mm. Afterwards, the supporting pressure reveals an overall larger value than that in the shallow-buried case due to its higher ground compression correspondingly.

We further investigate the movement of the ground at the tunnel face based on the DIC measurement. As depicted in Fig. 15, the displacement in sand and clay grounds shows an increasing trend as the moving of shield. Meanwhile, the deeply buried condition reveals an overall larger displacement at the tunnel face since heavier pressure concentration coming from the buried ground. For the shallow-buried case, the most evident ground movement occurs at the top position (#1) due to firstly the pressure concentration and secondly the lower cohesion of the sandy

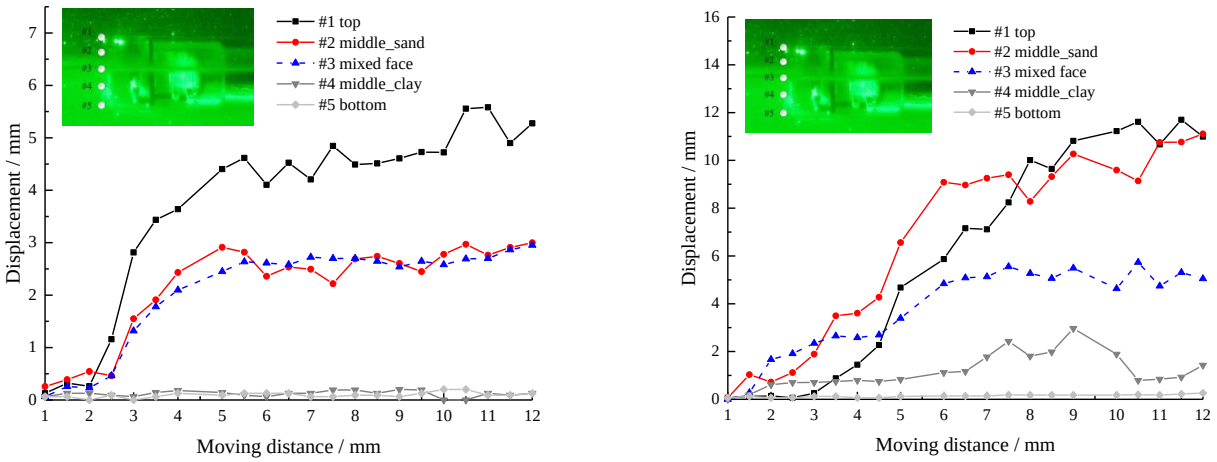

(a) shallow-buried case (C/D 1.0) (b) deep-buried case (C/D 2.0)

Fig. 15 Evolution of the ground displacement in front of the tunnel surface in two tunnels with a different buried depth. The mixed condition, buried depth and excavation distance influence a lot the displaced phenomenon of the ground

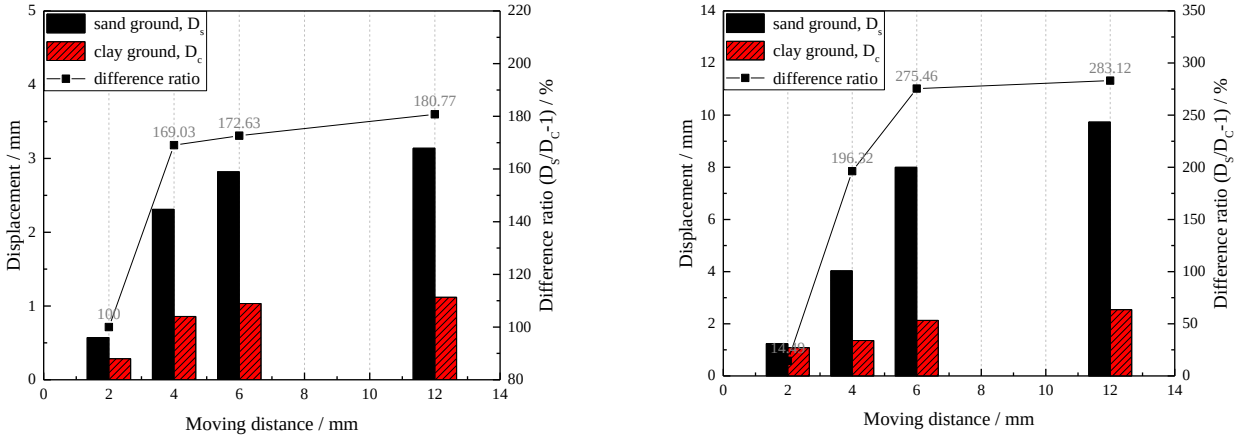

(a) shallow-buried case (C/D 1.0) (b) deep-buried case (C/D 2.0)

Fig. 16 Stratigraphic effect analysis of the ground displacement under mixed ground conditions. The stratigraphic effect is represented by the difference ratio of ground displacement of two points close to the mixed face in two respective materials

ground, and the top of the vault underwent a movement of 5.5 mm as the moving distance reaching 11 mm. However, for the deeply buried condition, the largest displacement at the excavation face initially occurs at the mixed face and gradually transfers to the upper area as can be seen from Fig. 15(b). Hence, we predict that a deeper buried condition induces a more dangerous ground movement in the mixed face in front of the tunnel head. For the bottom position, two cases show a similar movement around 0.2 mm throughout the excavation indicating an inactive response regarding the buried depth. We also note that the points below and above the mixed surface (#2 and #4) show quite different displacements in magnitude in two buried cases, and the difference of the displacement between #2 and #4 is also related to the buried depth.

4.4 Stratigraphic effect under the mixed-ground condition

To investigate the stratigraphic effect of ground displacement under mixed ground conditions, we draw the displacement phenomenon of two points above and below the mixed face, represented by D_s and D_c, respectively. It should be noted here two points are close to the mixed face that the distance (2 mm) to the mixed face is small compared with the tunnel diameter (40 mm), hence that the difference between the two values can indicate the stratigraphic effect. The stratigraphic effect is denoted by an index through a simple computation $(D_s/D_c - 1)$ with respective values around the mixed face.

Test data from the corresponding measurement points at moving steps of 2, 4, 6 and 12 mm were analysed to investigate the stratigraphic effect in the mixed ground, and the analysis results are shown in Fig. 16. The difference ratio of the ground displacement varies in a range from 100% to 180% for the shallow buried condition and 14% to 283% under the deep-buried condition, which illustrates the stratigraphic effect of the displacement distribution in the mixed ground. The ground displacement, as well as the difference ratio in the two cases, increases as the shield moving, indicating that the stratigraphic effect in the mixed ground is more distinct as proceeding of excavation.

Moreover, the deeply buried condition reveals a more remarkable stratigraphic effect reflected from a generally higher value of the difference ratio since the combined action of the rock strength and ground stress. Therefore, the localized ground displacement since the stratigraphic effect calls for a strengthened support solution for the mixed face and the buried depth needs to be considered as well in tunnelling practice facing the mixed ground condition.

5. Conclusions

This paper carried out physical modelling experiments of shield tunnels excavated under mixed ground conditions. Transparent soil surrogates which enable the optical measurement of internal deformation were innovatively used in this study to fabricate a mixed ground composed of simulated sand and clay. Based on the study, the following conclusions can be drawn:

(1) Two kinds of transparent soil showing different mechanical properties can be fabricated in layers to create mixed ground for modelling experiments. With the combination of DIC measurement and transparent material method, it is available to realize the visualization of internal deformation induced by tunnelling under mixed ground conditions which is hard to be achieved through conventional solutions.

(2) The deformation mode of ground in tunnel construction varies with the buried depth and mixed condition. In transparent soil experiments, the condition of uniformly sandy ground exhibits a conventional funnel-like region whose concentrated deformation starts from the bottom of the tunnel to the ground surface. Inconsistently, the shape and the scope of the damage zone under mixed ground condition change with the buried depth.

(3) The soil arching plays a role in tunnelling under mixed ground conditions which induces a funnel-like deformation zone. Particularly, the funnel boundary extends to ground surface under the shallow-buried condition inducing intenser ground settlement in comparison with the deep-buried case.

(4) Under mixed ground conditions, a deeper buried depth induces supporting pressure at the tunnel face falling at a higher speed and undergoing a larger change as the shield movement.

(5) A stratigraphic effect exists in tunnelling under mixed ground conditions that the ground movement in sand and clay region around the mixed face reveals a notable difference. The stratigraphic effect tends to be more obvious under deeper buried conditions.

Declaration

The authors declare that they have no known competing financial interests or personal relationships that could have appeared to influence the work reported in this paper.

Acknowledgements

The work was funded by the National Natural Science Foundation of China (52274141), National Key Research and Development Program of China (2022YFC3003304), Natural Science Fund for Colleges and Universities in Jiangsu Province (21KJB580004) and the Science and Technology Plan Project of Xuzhou, China (KC21310).

References

Alagha, A.S. and Chapman, D.N. (2019), "Numerical modelling of tunnel face stability in homogeneous and layered soft ground", *Tunn. Undergr. Sp. Tech.*, **94**, 103096. https://doi.org/10.1016/j.tust.2019.103096.

Chambon, P. and Corte, J.F. (1994), "Shallow tunnels in cohesionless soil: stability of tunnel face", *J. Geotech. Eng.*, **120**(7), 1148-1165. https://doi.org/10.1061/(ASCE)0733-9410(1994)120:7(1148).

Chen, R., Meng, F., Li, Z., Ye, Y. and Ye, J. (2016), "Investigation of response of metro tunnels due to adjacent large excavation and protective measures in soft soils", *Tunn. Undergr. Sp. Tech.*, **58**, 224-235. https://doi.org/10.1016/j.tust.2016.06.002.

Chen, R.P., Tang, L.J., Ling, D.S. and Chen, Y.M. (2011), "Face stability analysis of shallow shield tunnels in dry sandy ground using the discrete element method", *Comput. Geotech.*, **38**(2), 187-195. https://doi.org/10.1016/j.compgeo.2010.11.003.

Cui, Q.L., Wu, H.N., Shen, S.L., Yin, Z.Y. and Horpibulsuk, S. (2016), "Protection of neighbour buildings due to construction of shield tunnel in mixed ground with sand over weathered granite", *Environ. Earth Sci.*, **75**(6), 458. https://doi.org/10.1007/s12665-016-5300-7.

Galli, M. and Thewes, M. (2019), "Rheological characterisation of foam-conditioned sands in EPB tunneling", *Int. J. Civil Eng.*, **17**(1), 145-160. https://doi.org/10.1007/s40999-018-0316-x.

Ganiyu, A.A., Rashid, A.S.A. and Osman, M.H. (2016), "Utilisation of transparent synthetic soil surrogates in geotechnical physical models: A review", *J. Rock Mech. Geotech. Eng.*, **8**(4), 568-576. https://doi.org/10.1016/j.jrmge.2015.11.009.

Hasanpour, R., Schmitt, J., Ozcelik, Y. and Rostami, J. (2017), "Examining the effect of adverse geological conditions on jamming of a single shielded TBM in Uluabat tunnel using numerical modeling", *J. Rock Mech. Geotech. Eng.*, **9**(6), 1112-1122. https://doi.org/10.1016/j.jrmge.2017.05.010.

Hayashi H., Okazaki Y., Sakai D., Morimoto S. and Shinji M. (2022), "Numerical Analysis for Elucidating the Effect of Tunnel Excavation in Gravel-Mixed Ground", *Appl. Sci.*, **12**(3), 1667. https://doi.org/10.3390/app12031667.

Hird, C.C. and Stanier, S.A. (2010), "Modelling helical screw piles in clay using a transparent soil", *Proceedings of the 7th International Conference on Physical Modelling in Geotechnics*.

Keating, T.J., Wolf, P. and Scarpace, F. (1975), "An improved method of digital image correlation", *Photogrammetric Eng. Remote Sens.*, **41**(8), 993-1002.

Leca, E. and Dormieux, L. (1990), "Upper and lower bound solutions for the face stability of shallow circular tunnels in frictional material", *Géotechnique*, **40**(4), 581-606. https://doi.org/10.1680/geot.1990.40.4.581.

Lemer, A.C. (1997), "Old Cities and New Towns For Tomorrow's Infrastructure", *Civil and Structural Engineering* (chap. 4, pp. 73-88), https://doi.org/10.1016/B978-1-898563-33-4.50008-2

Li, B.Q. and Einstein, H.H. (2017), "Comparison of visual and acoustic emission observations in a four point bending

experiment on barre granite", *Rock Mech. Rock Eng.*, **50**(9), 2277-2296. https://doi.org/10.1007/s00603-017-1233-z.

Li, Y., Tang, X., Yang, S. and Chen, J. (2019), "Evolution of the broken rock zone in the mixed ground tunnel based on the DSCM", *Tunn. Undergr. Sp. Tech.*, **84**, 248-258. https://doi.org/10.1016/j.tust.2018.11.017.

Li, Y., Tang, X. and Zhu, H. (2022), "Optimization of the digital image correlation method for deformation measurement of geomaterials", *Acta Geotech.*, **17**, 5721-5737. https://doi.org/10.1007/s11440-022-01646-x.

Li, Y., Yang, S., Tang, X., Ding, Y. and Zhang, Q. (2020), "Experimental investigation of the deformation and failure behavior of a tunnel excavated in mixed strata using transparent soft rock", *KSCE J. Civil Eng.*, **24**, 962-974. https://doi.org/10.1007/s12205-020-0072-8.

Li, Y., Zhang, Q., Lin, Z. and Wang, X. (2016), "Spatiotemporal evolution rule of rocks fracture surrounding gob-side roadway with model experiments", *Int. J. Min. Sci. Technol.*, **26**(5), 895-902. https://doi.org/10.1016/j.ijmst.2016.05.031.

Liu, J. and Iskander, M. (2004), "Adaptive cross correlation for imaging displacements in soils", *J. Comput. Civil Eng.*, **18**(1), 46-57. https://doi.org/10.1061/(ASCE)0887-3801(2004)18:1(46).

Liu, J.Q., Yuen, K.V., Chen, W.Z., Zhou, X.S. and Wei, W. (2020), "Grouting for water and mud inrush control in weathered granite tunnel: A case study", *Eng. Geol.*, **279**, 105896. https://doi.org/10.1016/j.enggeo.2020.105896.

Ma, H., Yin, L., Gong, Q. and Wang, J. (2015), "TBM tunneling in mixed-face ground: Problems and solutions", *Int. J. Min. Sci. Tech.*, **25**(4), 641-647. https://doi.org/10.1016/j.ijmst.2015.05.019.

Meguid, M.A., Saada, O., Nunes, M.A. and Mattar, J. (2008), "Physical modeling of tunnels in soft ground: A review", *Tunn. Undergr. Sp. Tech.*, **23**(2), 185-198. https://doi.org/10.1016/j.tust.2007.02.003.

Sun, J. and Liu, J. (2014), Visualization of tunnelling-induced ground movement in transparent sand", *Tunn. Undergr. Sp. Tech.*, **40**, 236-240. https://doi.org/10.1016/j.tust.2013.10.009.

Tóth, Á., Gong, Q. and Zhao, J. (2013), "Case studies of TBM tunneling performance in rock–soil interface mixed ground", *Tunn. Undergr. Sp. Tech.*, **38**, 140-150. https://doi.org/10.1016/j.tust.2013.06.001.

Vergara, I.M. and Saroglou, C. (2017), "Prediction of TBM performance in mixed-face ground conditions", *Tunn. Undergr. Sp. Tech.*, **69**, 116-124. https://doi.org/10.1016/j.tust.2017.06.015.

Wang, J., Lin, G., Xu, G., Wei, Y., Li, S., Tang, X. and He, C. (2022), "Face stability of EPB shield tunnels in multilayered ground with soft sand lying on hard rock considering dynamic excavation process: A DEM study", *Tunn. Undergr. Sp. Tech.*, **120**, 104268. https://doi.org/10.1016/j.tust.2021.104268.

Wang, Q., Xie, X., Shahrour, I. and Huang, Y. (2021), "Use of deep learning, denoising technic and cross-correlation analysis for the prediction of the shield machine slurry pressure in mixed ground conditions", *Automat. Constr.*, **128**, 103741. https://doi.org/10.1016/j.autcon.2021.103741.

Xie, X., Wang, Q., Huang, Z. and Qi, Y. (2018), "Parametric analysis of mixshield tunnelling in mixed ground containing mudstone and protection of adjacent buildings: Case study in Nanning metro", *Eur. J. Environ. Civil Eng.*, **22**(1), s130-s148. https://doi.org/10.1080/19648189.2017.1359113.

Xu, Z.H., Wang, W.Y., Lin, P., Nie, L.C., Wu, J. and Li, Z.M. (2021), "Hard-rock TBM jamming subject to adverse geological conditions: Influencing factor, hazard mode and a case study of Gaoligongshan Tunnel", *Tunn. Undergr. Sp. Tech.*, **108**, 103683. https://doi.org/10.1016/j.tust.2020.103683

Xue, Y., Li, X., Qiu, D., Ma, X., Kong, F., Qu, C. amd Zhao, Y. (2019), "Stability evaluation for the excavation face of shield tunnel across the Yangtze River by multi-factor analysis", *Geomech. Eng.*, **19**, 283-293. https://doi.org/10.12989/gae.2019.19.3.283

Yang, H., Wang, H. and Zhou, X. (2016), "Analysis on the damage behavior of mixed ground during TBM cutting process", *Tunn. Undergr. Sp. Tech.*, **57**, 55-65. https://doi.org/10.1016/j.tust.2016.02.014.

Zhang, C., Han, K. and Zhang, D. (2015), "Face stability analysis of shallow circular tunnels in cohesive–frictional soils", *Tunn. Undergr. Sp. Tech.*, **50**, 345-357. https://doi.org/10.1016/j.tust.2015.08.007.

Zhang, P., Chen, R.P., Wu, H.N. and Liu, Y. (2020), "Ground settlement induced by tunneling crossing interface of water-bearing mixed ground: A lesson from Changsha, China", *Tunn. Undergr. Sp. Tech.*, **96**, 103224. https://doi.org/10.1016/j.tust.2019.103224.

Zhang, W., Gu, X., Zhong, W., Ma, Z. and Ding, X. (2020), "Review of transparent soil model testing technique for underground construction: Ground visualization and result digitalization", *Undergr. Space*, **7**(4), 702-723. https://doi.org/10.1016/j.undsp.2020.05.003.

Zhang, Z. and Huang, M. (2014), "Geotechnical influence on existing subway tunnels induced by multiline tunneling in Shanghai soft soil", *Comput. Geotech.*, **56**, 121-132. https://doi.org/10.1016/j.compgeo.2013.11.008.

Zhang, Z.X., Xu, Y., Kulatilake, P.H.S.W. and Huang, X. (2012), "Physical model test and numerical analysis on the behavior of stratified rock masses during underground excavation", *Int. J Rock Mech Min. Sci.*, **49**, 134-147. https://doi.org/10.1016/j.ijmst.2021.01.003.

Zhao, Y., Gong, Q., Tian, Z., Zhou, S. and Jiang, H. (2019), "Torque fluctuation analysis and penetration prediction of EPB TBM in rock–soil interface mixed ground", *Tunn. Undergr. Sp. Tech.*, **91**, 103002. https://doi.org/10.1016/j.tust.2019.103002.

IC